IEEE Access
Multidisciplinary | Rapid Review | Open Access Journal

Received July 18, 2018, accepted August 22, 2018, date of publication August 27, 2018, date of current version September 21, 2018.

Digital Object Identifier 10.1109/ACCESS.2018.2867228

Reverberation Chambers for Over-the-Air Tests: An Overview of Two Decades of Research

XIAOMING CHEN[1], (Member, IEEE), JIAZHI TANG[1], TENG LI[1], SHITAO ZHU[1], YUXIN REN[2], ZHIHUA ZHANG[2], AND ANXUE ZHANG[1]

[1]School of Electronic and Information Engineering, Xi'an Jiaotong University, Xi'an 710049, China
[2]Beijing Hwa-Tech Information System Co., Ltd., Beijing 100097, China

Corresponding author: Xiaoming Chen (xiaoming.chen@mail.xjtu.edu.cn)

This work was supported in part by the National Natural Science Foundation of China under Grant 61801366.

ABSTRACT The reverberation chamber (RC) has traditionally been used for electromagnetic compatibility tests. About two decade ago, it found application in various over-the-air (OTA) tests of antennas and wireless devices. This paper gives an overview of nearly two decades of research on the RC-based OTA tests, ranging from antenna measurements and characterizations to OTA tests of both terminals and base stations. Apart from the advantages of the RC-based OTA tests, some important issues are identified.

INDEX TERMS Antenna measurements, channel characterizations, over-the-air (OTA) tests, reverberation chamber (RC).

I. INTRODUCTION

The reverberation chamber (RC) is an electrically large cavity, where mechanical mode stirrers are employed to stir the electromagnetic field in order to create a random-like multipath environment (see Fig. 1). Due to the complicated test conditions, RC measurement results are usually studied from a statistical point of view. Hence it is vital to have a large number of independent samples to ensure accurate analysis of the measured data. Quite often a turn-table platform is used to increase the number of independent samples. For the same reasons, multiple fixed antennas (with sufficient separations or orthogonal polarizations) can be used as well.

The RC has traditionally been used for electromagnetic compatibility (EMC) tests [1]. Over the past two decades, the RC has found more and more applications in over-the-air (OTA) tests, such as measurements of antenna efficiency, reflection coefficient, radiation pattern, diversity gain, and multiple-input multiple-output (MIMO) capacity of passive antennas [2]–[23], and error rate, total radiated power (TRP), total isotropic sensitivity (TIS), and throughput of wireless devices [24]–[38]. Unlike EMC tests, active OTA tests (using either base station emulators [24]–[36] or a real base station [37], [38]) usually have specific requirements on the propagation channel (e.g., delay spread, Doppler spread, K-factor) in the RC. The delay spread (or coherence bandwidth) can be readily increased by loading the RC with lossy objects [39]. The Doppler spread (or coherence bandwidth) can be controlled by varying the speed of mode stirrers [25].

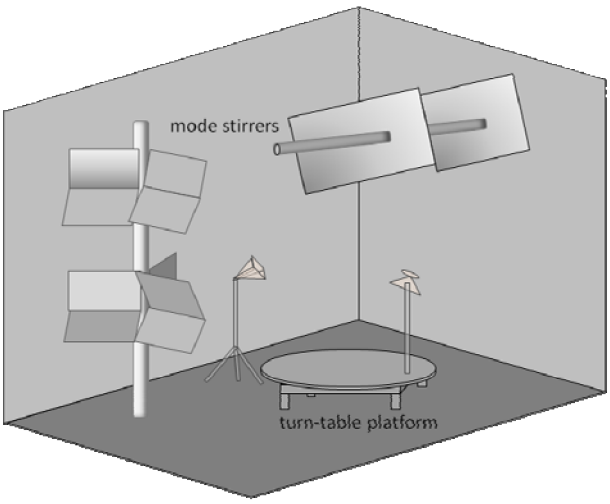

FIGURE 1. Illustration of an RC with two mode stirrers and one turn-table platform.

The K-factor can be controlled by loading the RC or rotating the directive antenna [40]. More sophisticated channels can be emulated by cascading the RC with a channel emulator [41]–[43]. However, care must be exerted to avoid the key hole effect [44].

Besides RC, multi-probe anechoic chamber (MPAC) [45] and radiated two-stage (RTS) [46] methods are another two popular OTA approaches that have been standardized in 3rd

generation partnership project (3GPP) and cellular telecommunication and Internet association (CTIA) for MIMO-OTA testing of MIMO terminals. The conventional MPAC approach can emulate two-dimensional (2D) MIMO channel in a small test area. Increasing the test area or extending it to 3D channel emulation will drastically increase the system cost. The RTS method can emulate 3D channel and has large test area. Nevertheless, it requires separate measurements of radiation patterns via a special chip in the device under test that may not be available in every device. By comparison, the RC is a cost-effective OTA approach that does not require separate measurements of radiation patterns and has large test area. The RC has been standardized in CTIA for OTA tests of large-form-factor devices [47]. However, a major drawback of the RC is its limited control of the power angular spectrum (PAS) of the emulated channel. It is usually regarded that the PAS in a well-stirred RC is statistically 3D isotropic [48]. Anisotropy can be achieved by partially covering internal walls of the RC with electromagnetic absorbers [49]–[51]. Nevertheless, to which extend the PAS can be emulated using this approach requires more investigation. Moreover, extra caution must be taken in that increasing the loading not only alters the channel characteristics but also degrades the measurement uncertainty of the RC [52].

This paper gives an overview of nearly two decades of research on the RC for OTA tests. State-of-the-art OTA tests are presented. Some open problems are identified. The rest of this paper is organized as follows. Section II introduces various measurements of antenna characteristics. Channel characterizations that are essential for active OTA tests are presented in Section III. Section IV describes various OTA tests of wireless devices for both terminals and base stations. Section VI concludes this paper.

II. ANTENNA MEASUREMENTS

The RC can be used to measure various free-space antenna characteristics.

A. MEASUREMENT OF ANTENNA EFFICIENCY

Different methods of measuring antenna efficiency in the RC exist in the literature. A standard method given by the international electrotechnical commission (IEC) involves a reference antenna with known efficiency [1]. For this reason, this method is referred to as the reference antenna method. In practice, the reference antenna with known efficiency may not be always available. As a result, various methods were proposed to get rid of the reference antenna. A time-reversal method was proposed in [3]. However, the method is applicable for ultra wideband antennas only. A reflection-based method was presented in [4]. Yet, the method result in coarse estimation due to measurement uncertainty in the return loss. By using two identical antennas under test, the antenna efficiency can be measured by estimating the quality factor of the RC [5]. Similarly, one-antenna, two-antenna, and three-antenna methods based on the quality factor measured from the time and frequency domains and the enhanced back scattering effect were presented in [6]. The methods proposed in [6] were referred to collectively as non-reference antenna methods [7].

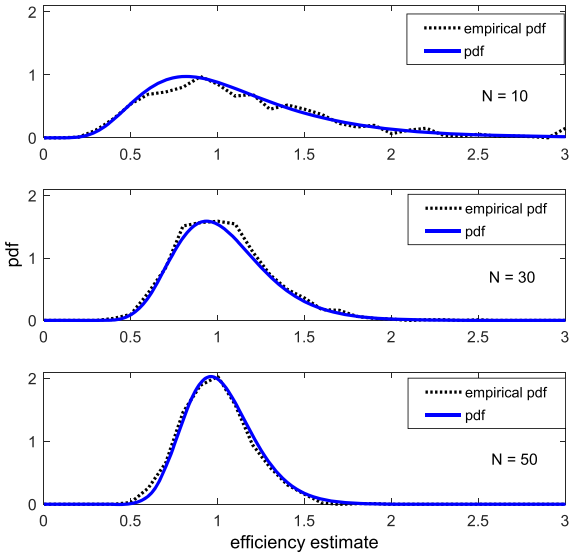

FIGURE 2. Comparisons of the analytical pdf (2) and the empirical pdf of estimated antenna efficiency with different number of independent samples [2].

1) REFERENCE ANTENNA METHOD

According to the reference antenna method [1], the antenna efficiency can be measured in an RC by first measuring the average power transfer function P_{ref} between a reference antenna (with known antenna efficiency e_{ref}) and a fixed antenna and then measuring the average power transfer function between the antenna under test (AUT) and the fixed antenna, P_{AUT}. During the measurements, both the reference antenna and the AUT should be placed in the RC so that the loading remains the same. The antenna efficiency of the AUT is obtained as

$$\hat{e}_{\text{AUT}} = \frac{\hat{P}_{\text{AUT}}}{\hat{P}_{\text{ref}}/e_{\text{ref}}} \tag{1}$$

where $\hat{e}_{\text{AUT}}$ is the measured value (estimate) of the antenna efficiency e_{AUT}, and $\hat{P}_{\text{AUT}}$ and $\hat{P}_{\text{ref}}$ are the estimates of P_{AUT} and P_{ref}, respectively.

Let $\hat{e}_{\text{AUT}} = e_{\text{AUT}}Z$, the probability density function (pdf) of Z can be derived as [2]

$$f_Z(z) = \frac{\Gamma(2N)}{(\Gamma(N))^2}\frac{z^{N-1}}{(1+z)^{2N}} \tag{2}$$

where Γ is the Gamma function, and N denotes the number of independent samples, which can be estimated from the measured samples [53]. Fig. 2 shows the empirical pdf of simulated $\hat{e}_{\text{AUT}}$ using Monte Carlo simulations against the theoretical pdf (2).

The mean and variance of $\hat{e}_{\text{AUT}}$ are [2]

$$\begin{aligned} E\left[\hat{e}_{\text{AUT}}\right] &= \frac{N}{N-1}e_{\text{AUT}}, \\ Var\left[\hat{e}_{\text{AUT}}\right] &= \frac{N(2N-1)}{(N-2)(N-1)^2}e_{\text{AUT}}^2, \end{aligned} \tag{3}$$

respectively. As can be seen, (1) is asymptotically unbiased and that $Var\left[\hat{e}_{\mathrm{AUT}}\right] \approx \frac{2}{N} e_{\mathrm{AUT}}^2$ for large N, which usually holds in practice. It is noted that the uncertainty analyses (2) and (3) assume the numbers of independent samples of the AUT and reference measurements are the same. For more general case where the numbers of independent samples of the AUT and reference measurements differ from each other was treated in [54].

2) NON-REFERENCE ANTENNA METHODS

The quality factor in the frequency domain is given as $Q_{FD} = \frac{16\pi^2 VP}{e_1 e_2 \lambda^3}$ [55], where V is the volume of the RC, $P = \left\langle |S_{21}|^2 \right\rangle$ is the average power transfer function, e_1 and e_2 are the antenna efficiencies of the two antennas, and λ is the free-space wavelength. The quality factor in the time domain is $Q_{TD} = \omega \tau_{RC}$, where ω is the angular frequency and τ_{RC} is the decay constant that can be extracted from the power delay profile of the RC [39]. Let $Q_{TD} = Q_{FD}$,

$$e_1 e_2 = \frac{16\pi^2 VP}{\omega \tau_{RC} \lambda^3}. \tag{4}$$

When the two antennas are identical, $e_1 = e_2 = e$, the antenna efficiency is

$$e = \sqrt{\frac{16\pi^2 VP}{\omega \tau_{RC} \lambda^3}} = \sqrt{\frac{16\pi^2 V \left\langle |S_{11}|^2 \right\rangle / e_b}{\omega \tau_{RC} \lambda^3}} \tag{5}$$

where $e_b = \left\langle |S_{11}|^2 \right\rangle / \left\langle |S_{21}|^2 \right\rangle$ is the enhanced backscatter coefficient [6].

The enhanced backscatter coefficient was found experimentally as $e_b = 2$ [56] (where intuitive explanations were given). Substituting $e_b = 2$ to (5), it is found that only one antenna is needed for the efficiency measurement, resulting the one-antenna method [6].

However, recently study shows that the enhanced backscatter coefficient varies over frequency and is sensitive to calibration issues, and is not exactly two [57].

To alleviate this problem, we assume $e_1 = e_2 = e_b$ but e_b does not need to be 2. It is easy to show in this case that $e_b = \sqrt{\left\langle |S_{11}|^2 \right\rangle \left\langle |S_{22}|^2 \right\rangle} / \left\langle |S_{21}|^2 \right\rangle$. The antenna efficiencies of the two antennas are

$$\begin{aligned} e_1 &= \sqrt{\frac{16\pi^2 V \left\langle |S_{11}|^2 \right\rangle / e_b}{\omega \tau_{RC} \lambda^3}} \\ e_2 &= \sqrt{\frac{16\pi^2 V \left\langle |S_{22}|^2 \right\rangle / e_b}{\omega \tau_{RC} \lambda^3}} \end{aligned} \tag{6}$$

respectively. Equation (6) is referred to as the two-antenna method [6]. A modified two-antenna method was proposed in [8], where the measurement accuracy of low antenna efficiency was improved.

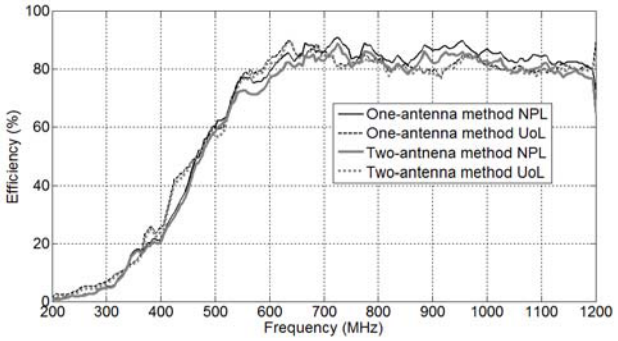

FIGURE 3. Comparisons of measured antenna efficiencies usign the non-reference antenna methods at different RCs [7].

To further relax the assumption on enhanced backscatter coefficients, we resort to three antennas such that

$$\begin{aligned} e_1 e_2 &= \frac{16\pi^2 V \left\langle |S_{21}|^2 \right\rangle}{\omega \tau_{RC} \lambda^3} \\ e_1 e_3 &= \frac{16\pi^2 V \left\langle |S_{31}|^2 \right\rangle}{\omega \tau_{RC} \lambda^3} \\ e_2 e_3 &= \frac{16\pi^2 V \left\langle |S_{32}|^2 \right\rangle}{\omega \tau_{RC} \lambda^3}. \end{aligned} \tag{7}$$

The antenna efficiencies are

$$\begin{aligned} e_1 &= \sqrt{\frac{16\pi^2 V \left\langle |S_{21}|^2 \right\rangle \left\langle |S_{31}|^2 \right\rangle}{\omega \tau_{RC} \lambda^3 \left\langle |S_{32}|^2 \right\rangle}} \\ e_2 &= \sqrt{\frac{16\pi^2 V \left\langle |S_{21}|^2 \right\rangle \left\langle |S_{32}|^2 \right\rangle}{\omega \tau_{RC} \lambda^3 \left\langle |S_{31}|^2 \right\rangle}} \\ e_3 &= \sqrt{\frac{16\pi^2 V \left\langle |S_{31}|^2 \right\rangle \left\langle |S_{32}|^2 \right\rangle}{\omega \tau_{RC} \lambda^3 \left\langle |S_{21}|^2 \right\rangle}} \end{aligned} \tag{8}$$

which is referred to as the three-antenna method [6].

The non-reference antenna methods were applied to efficiency measurements at different RCs. Reasonable agreements were observed (see Fig. 3) [7]. Recently, they have been applied for efficiency measurements of millimeter-wave antennas [11].

Unlike the reference antenna method, the distribution of the measured efficiency of the non-reference methods is still unknown. Therefore, the uncertainty analyses of the non-reference antenna methods were done empirically [6]. Nevertheless, as one step toward that direction, the distribution of the enhanced backscatter coefficient has been derived in [58].

B. MEASUREMENT OF ANTENNA IMPEDANCE

Use The free-space antenna impedance and reflection coefficient of an antenna can also be measured in the RC. It is shown that the measured S_{11} of an antenna at one state of the mode stirrer in an RC includes two parts: the free-space part and the stirred part (that is due to the scattering of

the RC) [13],

$$S_{11} = S_{11}^{fs} + S_{11}^{RC} \tag{9}$$

where S_{11} is the total reflection coefficient of the antenna in the RC, S_{11}^{fs} is the free space reflection coefficient, and S_{11}^{RC} is the scattering contribution from the RC. For a well stirred chamber, S_{11}^{RC} is a zero-mean complex Gaussian random variable. Thus, the ensemble average of S_{11}^{RC} over all the stirrer states $\langle S_{11}^{RC} \rangle$ should be close to zero.

Since the free space reflection coefficient does not depend on the stirrer state (and provided that there is enough independent stirrer states), the ensemble average of the reflection coefficient measured in the RC is

$$\langle S_{11} \rangle \approx S_{11}^{fs}. \tag{10}$$

In reality, the number of independent stirrer states in the RC is always limited. Thus, (10) is an approximation. In order to improve the estimation of S_{11}^{fs}, frequency stirring can be applied [59]. Nevertheless, the frequency stirring bandwidth must be selected judiciously. Increasing frequency stirring bandwidth (up to a certain value) will increase the number of independent samples so that $\langle S_{11} \rangle$ becomes closer to S_{11}^{fs}. Yet, a too large frequency stirring bandwidth will degrade the frequency resolution and the measurement accuracy.

The free-space reflection coefficient of a standard gain horn antenna was measured in an RC and in an anechoic chamber (AC). For a single frequency, 600 samples were gathered in the RC. The standard deviation (STD) of the error between the free-space reflection coefficients measured in the AC and RC was calculated. For this horn antenna specifically, the optimal frequency stirring bandwidth was found to be around 100 MHz. (Note that the optimal frequency stirring bandwidth depends on the antenna. For half-wavelength dipole antenna, the optimal frequency stirring is about 8 MHz [13].) Once the free-space reflection coefficient is obtained, the free-space antenna impedance can be readily determined. Fig. 4 shows the antenna impedance measured in an RC (with 100-MHz frequency stirring) and that measured in an AC. Very good agreement is observed.

It may seem redundant to measure the free-space reflection coefficient (or the free-space antenna impedance) in the RC, given the fact that it can be readily and accurately measured in the AC. However, most RC-based OTA tests are preferably done without the need of an AC. The free-space reflection coefficient extracted from the RC measurements is used to, e.g., calibrated out the channel transfer function that should be independent of antenna mismatches.

C. MEASUREMENT OF RADIATION PATTERN

Due to the strong scattering, it is usually believed that the RC is not suitable for measuring radiation patterns of antennas. Recently, radiation patterns have been successfully measured in the RC by using the K-factor [15]–[17] or Doppler shift [18]. For these kinds of measurements, a directivity antenna is oriented towards the AUT. The stirred fields are averaged out by rotating the stirrer [15]–[17] or filtered in the Doppler frequency domain (by moving the AUT along a straight line) [18]. However, the measurement times of these methods [15]–[18] are much longer than that of an AC measurement. The time-reversal technique can be used to measure the radiation pattern in the RC [19], where the RC needs to be carefully calibrated.

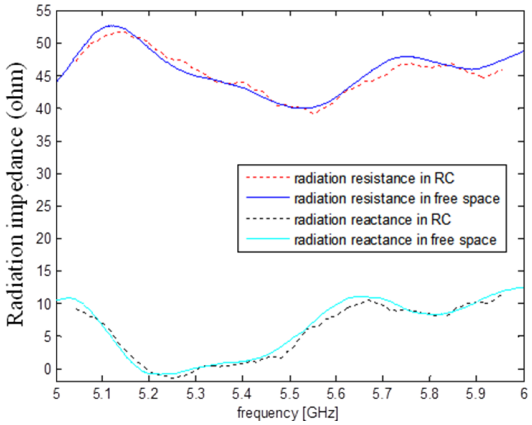

FIGURE 4. Comparisons of radiation resistances and reactances measured in RC and AC [14].

Very recently, Xu *et al.* [20] proposed a novel method for radiation pattern measurements, where the radiation pattern of the AUT is decomposed into spherical harmonics, whose unknown coefficients can be determined from the self-correlation coefficients (of the radiation pattern and the rotated version of itself) measured in the RC. The method relies on stirred components to obtain the self-correlation coefficients, instead of the unstirred component as [15]–[18]. As a result, the measurement time is significantly reduced. An example of the radiation pattern measured using the method [20] is plotted in Fig. 5. As can be seen, the co-polarized (CP) component of the radiation pattern can be accurately measured. However, there is noticeable error for the cross-polarized (XP) component of the radiation pattern. Finally, it is noted that the method becomes less efficient for non-directive AUT, where the number of levels of the spherical harmonic decomposition increases drastically.

In general, the radiation pattern measurement in the RC is not as accurate as that in the AC, despite the fact that the cost of an RC is much lower than that of an AC.

D. MEASUREMENT OF MIMO ANTENNAS

For MIMO antennas, apart from the traditional antenna characteristics, antenna correlation, diversity gain, and capacity are all important parameters. These parameters depend on not only the antenna characteristics but also the propagation channel, e.g., PAS and cross polarization discrimination (XPD) [60]. Nevertheless, due to the random orientation of the mobile handset, polarization balanced isotropic-scattering environments are usually assumed for characterizations of mobile antennas, rendering the RC a convenient test envi-

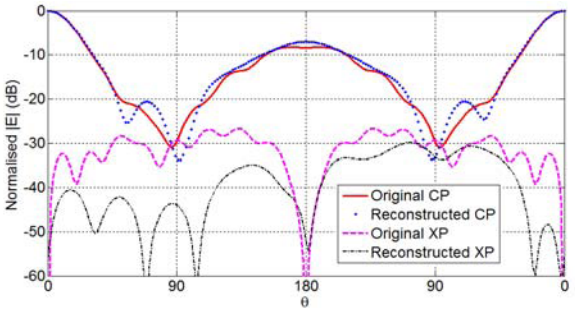

FIGURE 5. Comparison of measured radiation pattern against its true value [20].

ronment for measurements of handset MIMO antennas, e.g., [61].

1) CORRELATION MEASUREMENT

The signal correlation between the mth and nth antenna ports can be conveniently measured in the RC by following the definition of cross-correlation

$$\rho_{mn} = \frac{E[v_m v_n^*]}{\sqrt{E[|v_m|^2]E[|v_n|^2]}} \tag{11}$$

where v_m is the complex-valued signal received at mth antenna port. Note that the envelope correlation coefficient (ECC) (defined as the correlation between the signal envelopes) is often used instead of the signal correlation (11) in the antenna design literature. The ECC equals approximately squared magnitude of the signal correlation [62]. It is shown that the phases of the signal correlations can have profound effects on the MIMO performance (especially for spatial multiplexing) [63]. Moreover, the signal correlation can be directly incorporated in to the MIMO channel (e.g., in correlation-based channel models) [22]. Therefore, without specifications, (antenna) correlations used in the rest of this work means signal correlations.

The correlation can be calculated based on measured radiation patterns in the AC. Good agreements were observed between correlations measurements in the RC and AC (see Fig. 6) [22]. It is worth mentioning that the RC measurement is about 10 times faster than the AC measurement for a two-port MIMO antenna. Moreover, the difference of the measurement time increases with increasing number of antenna ports.

The correlation of MIMO antenna can be calculated from the free-space S-parameters even more conveniently [64]. However, the original method [64] is limited to lossless antennas. The S-parameter based correlation can be extended to lossy MIMO antenna by taking the antenna efficiency into account [65] with some uncertainty. The accuracy of this method was improved in [66] at the cost of increased complexity. Nevertheless, it is noted that both methods [65], [66] necessitate antenna efficiencies, whose measurement time in the AC is much longer than that in the RC.

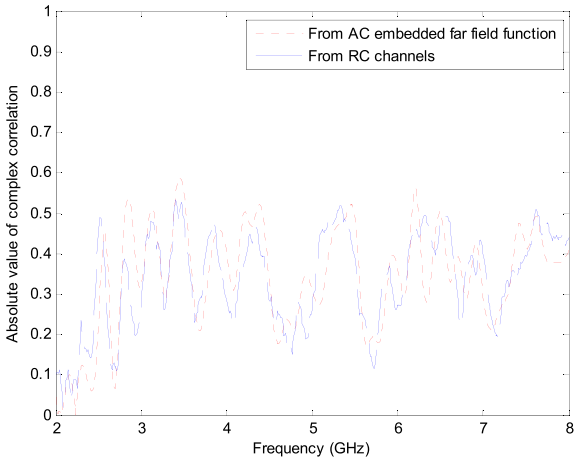

FIGURE 6. Comparison of correlations of a wideband two-port antenna measured in AC and RC [22].

2) MEASUREMENT OF DIVERSITY GAIN

The diversity gain of a multi-port antenna is defined as the signal-to-noise ratio (SNR) improvement of the multi-port antenna as compared to a single reference antenna at 1% cumulative distribution function (CDF) level [67]. It can be conveniently measured in the RC. The usage of the reference antenna can be avoided by using the two-antenna method [23].

The diversity gain is usually determined from the empirical CDF estimated from the channel samples. The problem is that, with limited independent channel samples in a practical RC, there can be high uncertainty at 1% CDF level. To avoid this problem, a so-called covariance eigenvalue approach was proposed in [22], where the theoretical CDF (derived by Lee [68]) was constructed using the eigenvalues of the covariance matrix of the diversity channel. Since the eigenvalues (in an well-stirred RC) depend only on the antenna efficiencies and correlations, the high uncertainty can be greatly alleviated. Nevertheless, when the number of independent samples is sufficiently large, both the covariance eigenvalue approach and the traditional method give the same result.

Note that the diversity gain depends on the actual diversity combining scheme. Figure 7 shows the diversity gains of a two-port ultrawideband antenna using selection combining (SC), equal gain combining (EGC), and maximum ratio combining (MRC) measured in an RC [69]. As can be seen, the MRC offers the highest diversity gain, whereas the SC results in the lowest diversity gain.

3) MEASUREMENT OF MIMO CAPACITY

Similar to the diversity gain, ergodic MIMO capacities of multi-port antennas can also be conveniently measured in the RC by measuring the MIMO channels [22],

$$C = E\left\{\log_2\left[\det\left(\mathbf{I} + \frac{\gamma}{M_t}\mathbf{H}\mathbf{H}^H\right)\right]\right\} \tag{12}$$

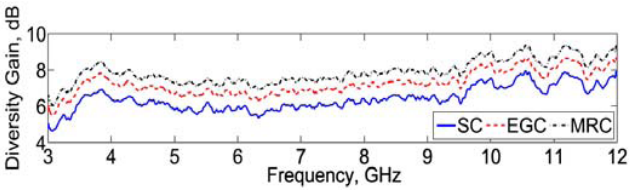

FIGURE 7. Measured diversity gains using various diversity combining schemes in an RC [69].

where γ is the SNR, E denotes the expectation, $\mathbf{I}$ is the identity matrix, M_t is the number of transmit antennas, $\mathbf{H}$ is the measured MIMO channel matrix normalized by the square root of the average power transfer function (measured by a reference antenna).

For modest MIMO size, the MIMO channel in the RC can be well approximated by the Kronecker channel model

$$\mathbf{H}_{Kron} = \mathbf{R}_r^{1/2}\mathbf{H}_w\mathbf{R}_t^{1/2} \tag{13}$$

where $\mathbf{R}_t$ and $\mathbf{R}_r$ are covariance matrices at the transmit and receive sides, respectively, $\mathbf{R}_r^{1/2}\left(\mathbf{R}_r^{1/2}\right)^H = \mathbf{R}_r$, $\mathbf{H}_w$ is independent and identically distributed (i.i.d.) zero mean Gaussian matrix. Using the Kronecker model (with measured antenna efficiencies and correlation in the AC), the capacities of MIMO antennas can be obtained based on AC measurements. Good agreement was observed between the capacity measurements in RC and AC [22].

Surprisingly, as the number of antennas increases, the elements in the MIMO channel are not jointly Gaussian any more. This holds, in particular, for orthogonally polarized antennas [70]. Certain effort has been exerted to explain this phenomenon using the random coupling model [71]. Unfortunately, to date a theoretical explanation of the underlying mechanism is still missing.

III. CHANNEL CHARACTERIZATIONS

If Channel characterizations are vital for active OTA tests. In general, the radio channel is a function of angle, time, and delay $h(\Omega_\mathrm{r}, \Omega_\mathrm{t}, t, \tau)$, where t is the time, τ is the (time) delay, and Ω_r and Ω_t are the (solid) angle of arrival (AoA) and angle of departure (AoD), respectively [72], [73]. We characterize the channel in each domain separately in the sequel.

A. FREQUENCY AND DELAY DOMAINS

The Fourier transform of the channel impulse response $h(\tau)$ is the channel transfer function $H(f)$. Hence, $h(\tau)$ contains the same information as $H(f)$ and channel characterizations in frequency domain and delay domain are inter-related. The coherence bandwidth B_c is used to evaluate the frequency selectivity of a multipath channel, while the root mean square (RMS) delay spread σ_τ is used to characterize the time dispersiveness of the channel [74]. When the system bandwidth is much smaller than B_c, the channel is called frequency-flat. Otherwise, when the system bandwidth becomes comparable or even larger than B_c, the channel is referred to as frequency-selective.

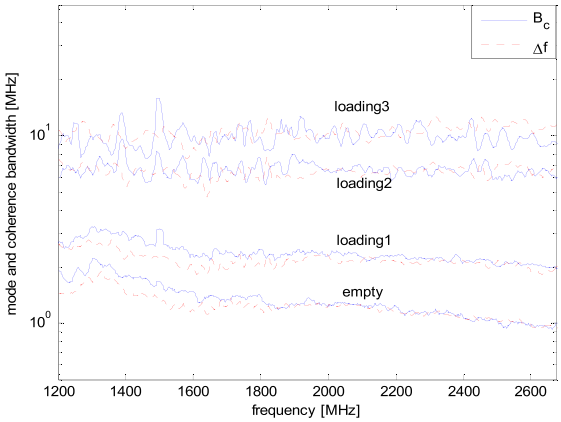

FIGURE 8. Comparison of average mode bandwidths and coherence bandwidths under different RC loadings [39]. (The loading increases from "loading1" to "loading3".)

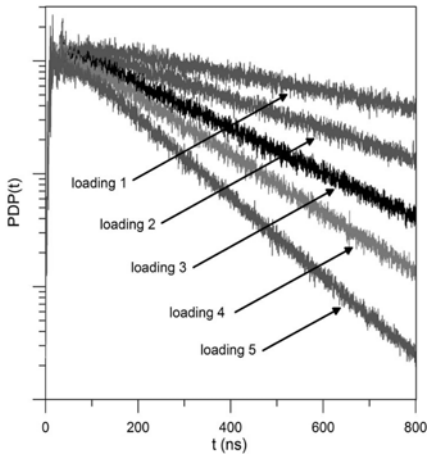

FIGURE 9. Measured power delay profile (PDP) in an RC under different loading conditions [77].

The distribution of B_c in the RC was derived in [75]. It was shown that B_c equals approximately the average mode bandwidth and $B_c = \sqrt{3}/(2\pi\sigma_\tau)$ in a well-stirred RC [39], where B_c is defined as half-bandwidth of the (normalized) autocorrelation function (ACF) of $H(f)$ with a threshold of 0.5. By increasing the RC loading, the coherence bandwidth increases (see Fig. 8) and the delay spread decreases (see Fig. 9). Thus, the RC loading has become a standard method for tuning the RC for active OTA tests [47]. Nevertheless, it is found that the actual location of the loading also affects the delay spread. As a result, a specific RMS delay spread (or coherence bandwidth) was usually achieved by using try and error in loading the RC. Fortunately, Dortmans *et al.* [76] proposed a method that gives guidelines on RC loading to obtain specific tuning. According to the method, the S-parameters of an unloaded RC and that of the RC loaded with absorbing blocks of a known amount of exposed surface area are measured sequentially. The amount of absorbing blocks needed to obtain the desired tuning can be readily

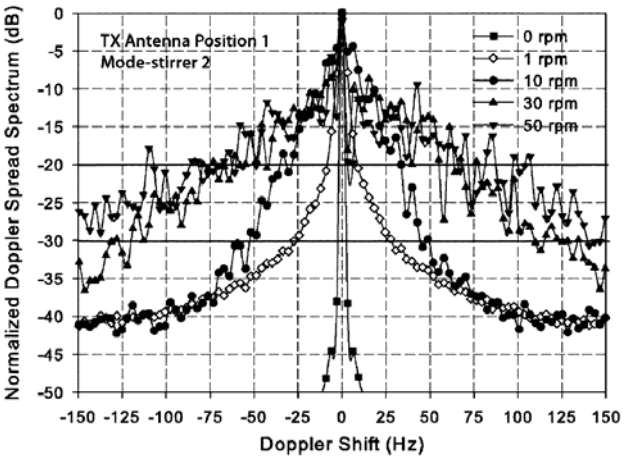

FIGURE 10. Measured Doppler spectra under different mode stirrer speeds [78].

calculated afterwards. In this way, the RC tuning time can be reduced significantly.

B. TEMPORAL AND DOPPLER DOMAINS

Similarly, the channel is characterized using coherence time T_c in the time domain and RMS Doppler spread σ_D in the Doppler frequency domain. T_c is inversely proportional to σ_D. When the symbol duration is much smaller than T_c, the channel is called slow fading. Otherwise, when the symbol duration becomes comparable or even larger than T_c, the channel is referred to as fast fading. In general, the Doppler spread increases with increasing carrier frequency and/or moving speed. The Doppler spread in the RC has been studied empirically in [78] by measuring the time-varying channel using a channel sounder. The conventional time-domain measurement of the Doppler spread is limited to the carrier frequency and actual stirring speed, at which the time-varying channel is measured. The Doppler spread at another carrier frequency or stirring speed needs to be characterized by another measurement. Karlsson *et al.* [79] proposed a so-called stepwise stationary stirring method, where the channel is measured stepwise at predefined stirring positions. The time-varying channel is then obtained by transforming the static channel samples from the spatial domain to the time domain with a virtual speed in post-processing. The Doppler spectrum can then be estimated as the Fourier transform of the ACF of the time-varying channel or the square magnitude of the Fourier transform of the time-varying channel [79]. Using the stepwise stationary stirring method, the Doppler spread at any carrier frequency (within the measured bandwidth) and any stirring speed can be obtained via prost-processing of a vector network analyzer (VNA) based measurement.

Anyway, it has been shown that the Doppler spread increases with increasing mode stirrer speed. As a demonstration, Fig. 10 shows the measured Doppler spectra under different mode stirrer speeds in an RC [78].

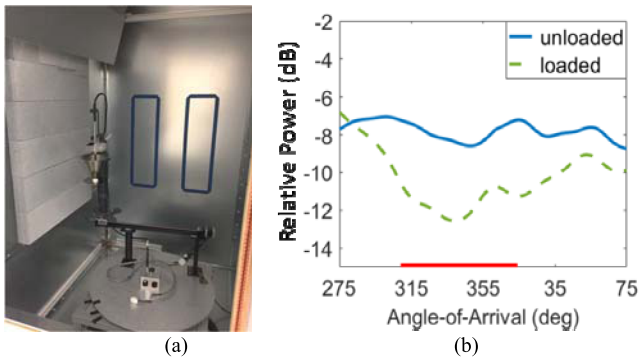

FIGURE 11. (a) Loading configuration. (b) PASs with and without loading [51].

C. SPATIAL AND ANGULAR DOMAINS

To be exact, the Fourier transform of the spatial-domain channel is the wave vector domain channel. The wave vector can be expressed as $\mathbf{k} = \left(k\cos\theta\sin\varphi,\ k\cos\theta\cos\varphi\right)$, where k is the scalar wave number, θ and φ are the elevation and azimuth angles, respectively. Thus, the wave vector domain and angular domain are usually used interchangeably in the channel sounding literature. That is the angular-domain channel can be obtained from the spatial-domain channel via Fourier transform.

By decomposing the electromagnetic modes in the RC into plane waves, it was shown that the incident waves in the RC are 3D uniformly distributed [48]. Nevertheless, perfect mechanical stirring and narrowband channel were implicitly assumed in [48]. In practice, the statistical isotropy cannot be perfectly achieved, especially at low operating frequencies [80]. More importantly, as the bandwidth increases (i.e., the delay resolution improves), waves arriving at different delays become separable. That is, the number of incoming waves at distinguishable delay bin reduces as the bandwidth increases. Hence, it is expected that the practical RC shows certain degree of statistical anisotropy, especially for broadband communications.

The PAS in the RC has been studied in [49]–[51] and [81]. The PAS in the RC was measured by simply rotating a horn antenna in [49]. Yet, this method suffers from poor angular resolution due to the limited aperture of the horn antenna. The multiple signal classification (MUSIC) algorithm was used to estimate the angular spectrum of a small RC loaded with large absorbers [50]. However, the MUSIC algorithm dictates that the number of incident angles should be smaller than the number of array elements. Thus, the method can be challenging for large RC with modest loading. By Fourier transforming the spatial domain samples to the angular domain, it is shown in [51] that the PAS can be controlled by covering the wall in the RC with absorbing materials (see Fig. 11). The Fourier transform of the spatial array elements is equivalent to the conventional beamformer, whose beamwidth varies with frequency. As a result, the obtained power angle delay profile becomes less accurate, since the beam of the sounding array varies with frequency. A promising method for estimating the

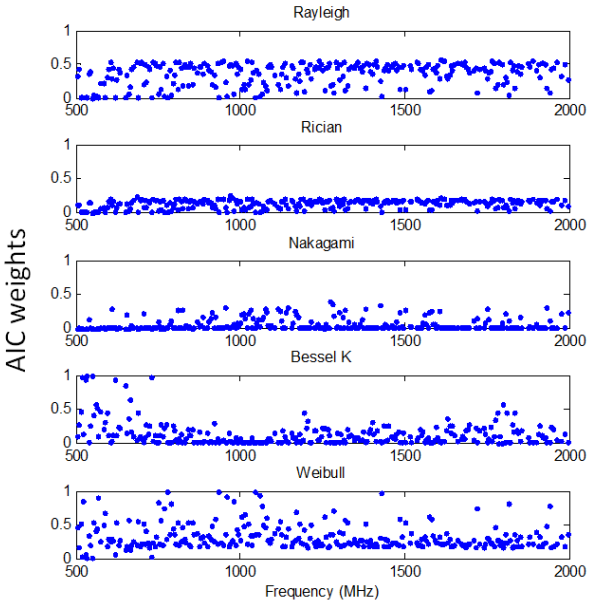

FIGURE 12. Comparison of AIC weights for Rayleigh, Rician, Nakagami, Bessel K, and Weibull distributions of an unloaded RC [89].

RC's angular spectrum is the so-called frequency invariant beamforming (FIB) algorithm [82], [83] by using the antenna on the turn-table platform [84] as a synthetic circular array.

As mentioned before, a major drawback of the RC for MIMO-OTA testing is the limited control of PAS in the RC. The work in [51] was intended to address this important issue. Yet, to which degree the PAS of the standard MIMO-OTA channel model, e.g., the spatial channel model extended (SCME) [85], can be emulated by RC loading deserves more investigations. Moreover, since loading will inevitably increase the measurement uncertainty [52], extra cautions must be taken when loading the RC with absorbers.

D. CHANNEL DISTRIBUTION

Due to the central limit theorem, the channel coefficients in a well-stirred and overmoded RC follows Gaussian distribution. Depending on the RC loading or antenna orientations, the channel magnitude can be Rayleigh or Rician [40], [86], [87]. When the operating frequency is below or close to the lowest usable frequency [88] (i.e., the RC is operating near the undermoded region), the channel coefficients do not follow Gaussian distribution any more.

The Akaike's information criterion (AIC) approach was used to study the channel distribution by comparing the measured channel in an RC with Rayleigh, Rician, Nakagami, Bessel K, and Weibull distributions [89]. The AIC weights represents relative feasibilities of the distribution candidates, ranging from zero (the worst fit) to one (the best fit). Figure 12 shows the AIC weights of different distribution candidates as a function of operating frequency in an unloaded RC (where non-directive antennas were used). The LUF of the used RC is around 700 MHz. As can be seen, above the LUF, the channel coefficients follow Rayleigh distribution as expected. Below the LUF, Bessel K and Weibull distributions tend to fit the measured channel better, which will become clearer for loaded RC.

IV. OTA TESTS OF WIRELESS DEVICES

The RC has be used to measure the TRP [28] and TIS [29] of mobile phones almost fifteen years ago. Since the era of the long term evolution (LTE), throughput becomes a more popular performance metric for LTE terminals [31]. Recently, there is a strong need for OTA tests of base stations. Relevant metrics are adjacent channel leakage power ratio (ACLR), carrier aggregation, etc. In this section, we discuss these active OTA tests separately.

A. TRP AND TIS

TRP and TIS are fundamental metrics for the emerging machine-to-machine (M2M) and wireless-internet-of-things (W-IOT) devices. TRP tests of a large-form-factor M2M device in an RC has been successfully demonstrated for the first time in [32], offering strong support for the CTIA standardization of using RC for OTA tests of large-form-factor devices [47].

A typical setup of the TRP and TIS measurements is shown in Fig. 13. As mentioned before, RC loading is often needed to tune the RC to reach a certain RMS delay spread. Prior to actual measurements of the device under test (DUT), a reference antenna is used to measure the average power transfer function (i.e., reference measurement) in the RC (similar to that in the reference antenna method of efficiency measurement in Section II-A-1).

For TRP tests, the communication tester (i.e., base station emulator) first establish an OTA connection to the DUT and control it to radiate at its maximum output power, and then measure the power sample at each mode-stirring state. (It is noted that, in the early versions of the communication tester, a power meter or spectrum analyzer was used to gather the power samples. In this case, the power meter or spectrum analyzer must be connected via a calibrated power splitter. Nowadays, the power meter is usually integrated into the communication tester, eliminating the trouble of having a separate instrument for TRP measurements.) The TRP is finally calculated as

$$TRP = \frac{1}{P_{ref}} \frac{1}{M} \sum_{m=1}^{M} P_m \tag{14}$$

where M is the number of samples, P_m is the power sample at the mth mode-stirring state, and P_{ref} is average power transfer function (including transmission loss, cable loss, mismatch, etc.) from the reference measurement.

For TIS tests, the communication tester first establish an OTA connection to the DUT and set it in the loopback mode for error rate measurement. Increase or decrease the output power of the communication tester until the lowest output power for a specified error rate target is found and recorded. The same procedure is repeated at each mode-stirring state.

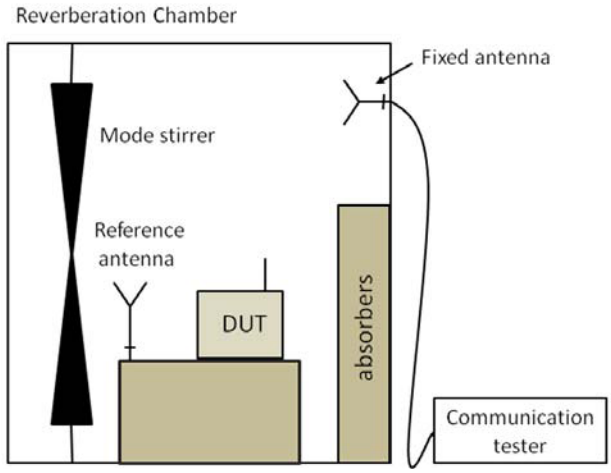

FIGURE 13. Measurement setup of TRP and TIS tests.

The TIS is finally calculated as

$$TIS = P_{ref} M \left(\sum_{m=1}^{M} \frac{1}{\tilde{P}_m} \right)^{-1} \tag{15}$$

where $\tilde{P}_m$ is the lowest output power sample of the communication tester at the mth mode-stirring state where the error rate target is met. Unlike the TRP which is the arithmetic mean of the samples, the TIS is the harmonic mean of the samples.

Since the standard TIS measurement described above requires a power search at each of the mode-stirring states, the TIS measurement can be quite time-consuming. It was found recently that the TIS of LTE devices can be extracted from throughput measurement that is much faster than the TIS measurement [35].

B. THROUGHPUT

Throughput has been chosen as the standard performance metric for MIMO-OTA tests. A typical setup of the throughput measurement is shown in Fig. 14. Typically, the RC is loaded so that the RMS delay spread equals 80 ns. The RC is set to the continuous stirring mode. And a reference measurement is performed a priori. For the actual throughput measurement, the communication tester first establish an OTA connection to the DUT and transmit data to it. The DUT sends back positive acknowledgment (ACK) for correctly received data block and negative acknowledgement (NACK) for erroneous data block. The throughput is then calculated at the communication tester based on the ACKs and NACKs. This procedure is repeated many times to get an average of the throughput at each average power level.

The DUT (i.e., a commercial LTE mobile phone) used in the tests was connected with the good, nominal, and bad CTIA reference antennas [90]. The CTIA reference antennas include electromagnetic shielding boxes in which DUT was placed. The magnitudes of the antenna correlations of the good, nominal, and bad CTIA reference antennas are about 0.13, 0.57, and 0.90, respectively. The antenna efficiencies of the good, nominal, and bad CTIA reference antennas are

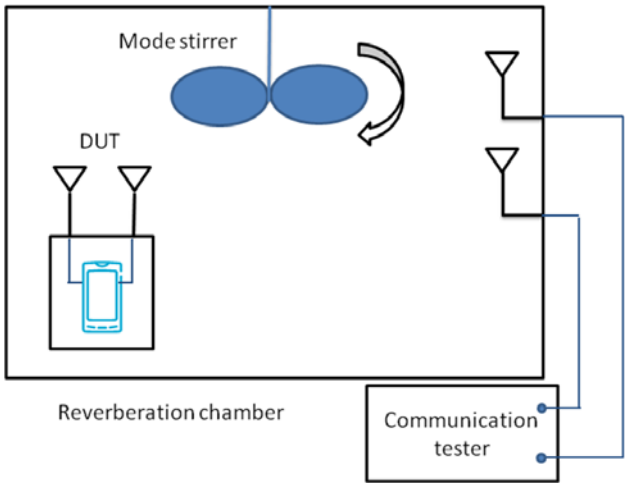

FIGURE 14. Measurement setup of 2 × 2 MIMO throughput tests.

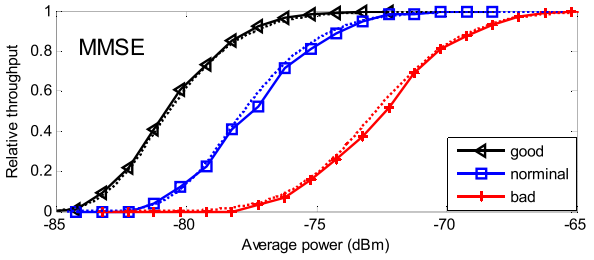

FIGURE 15. Relative throughputs of 2 × 2 LTE MIMO system. Good, nominal, and bad denotes the good, nominal, and bad CTIA reference antennas, respectively. Solid curves represent measurements; dotted curves represent the throughput models [36].

about −1.4, −3.1, and −4.0 dB, respectively. The throughput measurements were performed on the LTE band 13, i.e., 751 MHz, with 10-MHz system bandwidth. The communication tester was set to a fixed 64 QAM modulation with maximum rates of about 35 Mbps in the spatial multiplexing mode. The measurement results are shown in Fig. 15.

In order to double check the measurements and offer insight into the throughput tests, a throughput model was first proposed for single-input multiple-output (SIMO) LTE systems in [31]. The model was extended to the MIMO spatial multiplexing in [36]. For comparison, the simulated throughputs are also plotted in Fig. 15, where excellent agreements between measurements and simulations are observed. Very recently, the throughput model was extended to MPAC and RTS testing environments [91].

C. ACLR

The ACLR is also known as the adjacent channel power ratio (ACPR). There is usually an requirement on the maximum value of ACLR of a base station in order to reduce interferences to adjacent channels [92]. In practice, the nonlinearity of the radio frequency (RF) component, e.g., power amplifier (PA), causes not only in-band distortion but also out-of-band (OOB) emission, resulting in an increase of the ACLR.

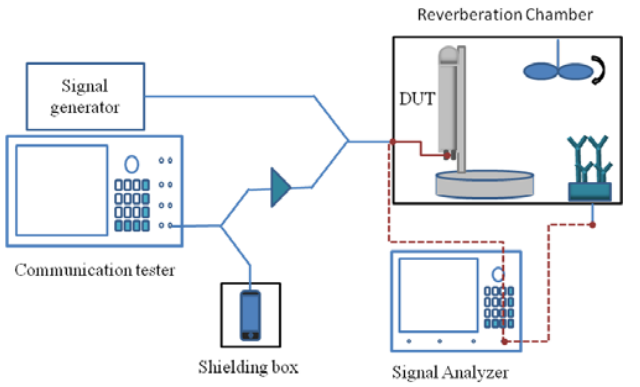

FIGURE 16. OTA testing setup of ACLR.

Traditionally, the ACLR was measured conductively at the antenna connector. However, it is shown that even modest mutual coupling (e.g., −15 dB) of the MIMO antenna in combination of PAs can cause severe OOB emission [93]. Obviously, the conductive measurement of ACLR cannot capture this phenomenon. Furthermore, in the fifth generation (5G) communications, massive MIMO and millimeter-wave (mmWave) techniques will be used. Massive MIMO base station antenna has hundreds of antenna ports, making the conductive test a formidable task. Due to cost, limited physical space, and high insertion loss, it is very likely that 5G mmWave systems will not have standard antenna ports, which makes conductive tests infeasible. Therefore, in 5G, OTA tests will not be optional any more [94]. As a result, OTA testing is needed for ACLR measurements of both 4G and 5G base stations.

An OTA testing setup of the ACLR has been demonstrated in the RC [95]. Figure 16 shows the measurement setup. The communication tester is connected to a mobile phone and a PA via a power splitter. The mobile phone is located in a shielding box to avoid interference. Since the signal output from the communication tester is very linear, the PA is used to introduce nonlinearity to mimic the real-life scenario. In addition, a continuous wave is generated from the signal generator to emulate spurious signal, which is combined with the output signal from the PA and fed to the antenna port of the base station antenna. The radiated power samples from the base station antenna are measured and recorded using the signal analyzer during continuous stirring (similar to the TRP test). The power samples are averaged over the bandwidths of the target and adjacent channels, and the ACLR is calculated as the ratio of the power in the adjacent channels to the power in the target channel.

D. CARRIER AGGREGATION

As an important feature of the LTE-advanced (LTE-A), the aggregation of more frequency carriers, i.e., carrier aggregation (CA) allows more efficient use of the frequency resources and, therefore, higher throughput. Recently, the first OTA test of the CA of a real LTE base station was conducted

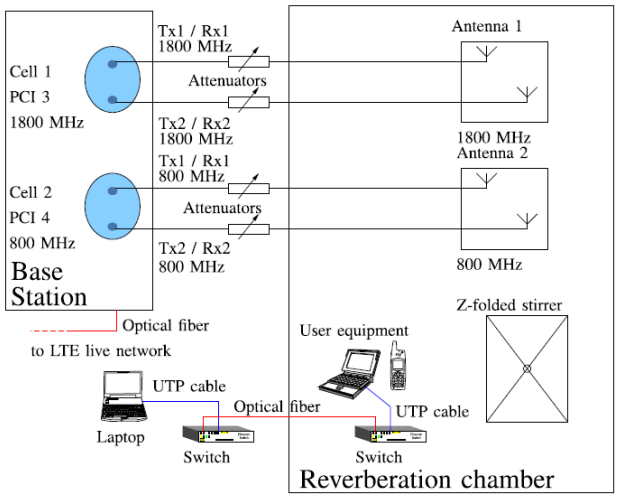

FIGURE 17. Measurement setup of carrier aggregation [96], where a real base station (connected to the live LTE mobile operator network) was tested.

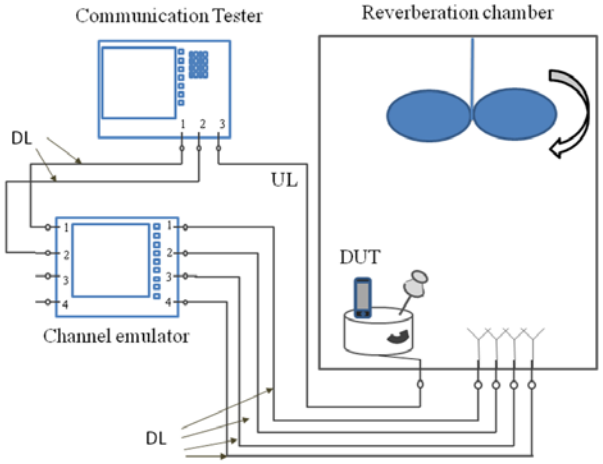

FIGURE 18. Measurement setup of RC in combination of CE.

in an RC [96]. Figure 17 shows the measurement setup. Two carriers were selected for aggregation: one at 800 MHz with 10-MHz bandwidth and the other at 1800 MHz with 20-MHz bandwidth. The two carriers were from two different cells. The downlink MIMO transmission was enabled on both cells, each corresponds to two antenna ports. The base station was located outside the RC. The antenna ports of the base station were connected to two dual-port MIMO antennas in the RC via RF cables. An LTE mobile phone prototype was used to establish data connection to the base station. (The laptop was left unused.) The CA performance was measured in terms of throughput, reference signal received power (RSRP), block error rate (BLER), and the channel quality indicator (CQI). Measurement results showed that the CA improves the throughput, RSPR, and CQI, while keeping a similar BLER as that of the primary cell (without CA).

E. RC COMBINED WITH CHANNEL EMULATOR

In order to enhance the flexibility of channel emulations, the RC can be combined with a channel emulator (CE) [41]–[43]. Figure 18 shows the measurement setup of the RC combined with a CE for OTA tests of a 2 × 2 MIMO system. The two output ports of the communication tester are connected with two input ports of the CE, which is then further connected to four fixed antennas in the RC via RF cables. By programming the CE, more sophisticated channels with complex power delay profiles and Doppler spectra can be emulated. (For instance, it is shown that the power delay profile of the 3GPP channel model [85] can be well emulated by cascading the RC with an CE [42], [43].) The spatial characteristics at the base station side is fully controllable by the CE, whereas the user (DUT) side is statistically isotropic.

It is noted that, four RF cables are used to connect four output ports from the CE to four fixed antenna in the RC for OTA testing of a 2 × 2 MIMO system. This is needed to overcome the key hole (or Double Rayleigh) effect [44], which causes an unintentional rank reduction of the MIMO channel in OTA tests. For OTA testing of a high order MIMO system (e.g., 4 × 4 or 8 × 8), more RF cables between the CE and the RC are needed.

The combination of RC with CE increase the degree of freedom in channel emulation. However, it also drastically increases the cost of the RC-based OTA system. Given the facts that cost effectiveness is one of the biggest advantage of the standalone RC OTA solution and that the RC plus CE solution offers limited control of the spatial characteristics at the DUT side, the standalone RC has been recently chosen as standardized solution for OTA testing of large-form-factor devices [47].

F. CHANNEL IMPACTS ON OTA TESTS

As mentioned before, the channel characteristics can have profound impacts on OTA tests. By loading the RC with condensed absorbing materials, the coherence bandwidth (delay spread) can be increased [39]. To show the coherence bandwidth effect on OTA tests, LTE throughput measurements with different system bandwidths were conducted under different loading conditions [35]. Figure 19 shows the measured throughputs as a function of average received power. As can be seen, it is beneficial for the LTE system to operate in a more frequency-selective channel, provided that the OFDM cyclic prefix is longer than the delay spread. This is because that, for a fixed system bandwidth, the number of independent OFDM subcarriers increases as the coherence bandwidth decreases, resulting in larger frequency diversity order (i.e., stepper throughput curve).

The RC loading not only changes the frequency selectivity of the channel but also alters the angular spectrum (see Fig. 11), which in turn incurs an impact on the Doppler spectrum. Figure 20 shows Doppler spectra of an RC with the same mode-stirring speed yet under different loading conditions. As can be seen, the Doppler spread reduces with

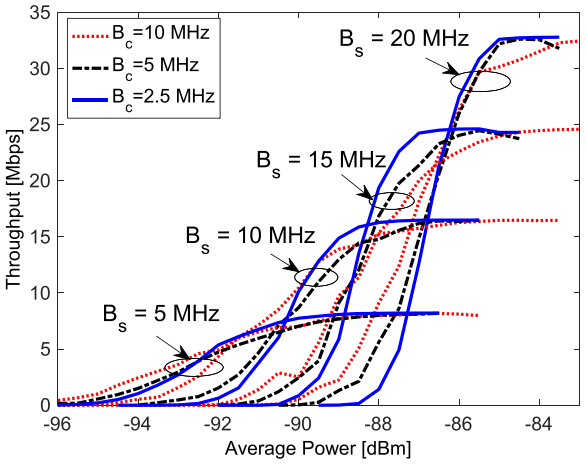

FIGURE 19. Throughput measurements of an LTE device with system bandwidths of 20, 15, 10, and 5 MHz and coherence bandwidths of 10, 5, and 2.5 MHz, respectively.

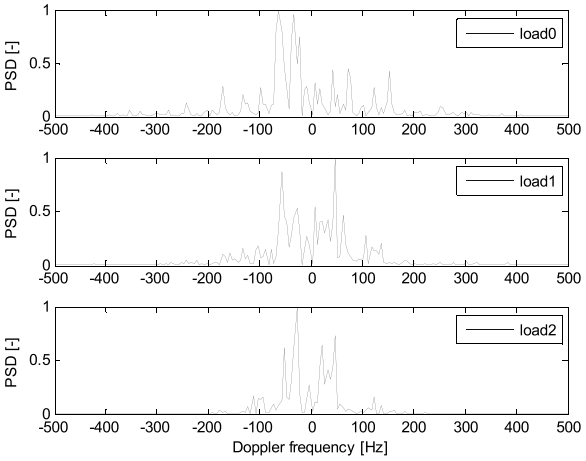

FIGURE 20. Doppler spectra under different RC loading.

increasing loading. This is because that Doppler spectrum consists of different Doppler frequency shifts from different incident angles (i.e., different relative velocities). As the loading increases, the number of incident wave decreases, resulting in a shrinking of the Doppler spread.

To show the Doppler effect on OTA tests, the package error rate (PER) of IEEE 802.11p nodes was measured in an RC with different mode-stirring speeds [25]. The corresponding results are shown in Fig. 21. As can be seen, as the mode-stirring speed increases from speed 1 to speed 3, the PER performance degrades gradually. This is because that, as the mode-stirring speed increase, so does the Doppler spread, which gradually destroys the orthogonality of the OFDM waveform used in the 802.11p. Moreover, it is more difficult to estimate the channel accurately as the time-variation increases and the estimated channel becomes outdated more easily due to the time-varying channel, rendering poor channel equalization and, therefore, poor PER. Therefore, it has been observed that the error rate performance of the single-carrier waveform also degrades as the stirrer speed increases [97].

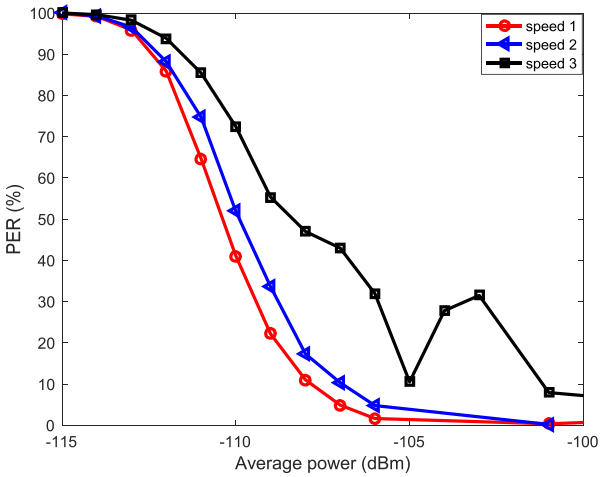

FIGURE 21. PERs of 802.11p under different mode-stirring speeds.

As can be seen, the channel may have profound impacts on OTA tests. Therefore, prior to OTA testing, the channel in the RC must be tuned carefully to make sure that the DUT is operating in certain channel conditions and that OTA tests in different RC labs are comparable.

G. MEASUREMENT UNCERTAINTY OF OTA TESTS

Since the RC measurements are in essence (quasi-)stochastic measurements, it is important to analyze the measurement uncertainty of the RC-based OTA tests and, more importantly, reduce the measurement uncertainty by carefully configuring the RC. One can estimate the effective number of independent samples [98]–[100], which is related to the measurement uncertainty (i.e., a larger number of independent samples implies a smaller measurement uncertainty). Convenient as it is, the number of independent samples offers limited insight into the mechanisms for measurement uncertainty. By separating the stirred and unstirred components of the field in the RC, it was shown that the K-factor represents a residual error and that the measurement uncertainty can be improved by minimizing the K-factor (or direct coupling) [52]. Consequently, a K-factor based uncertainty model was proposed and verified by extensive measurements in [52]. The uncertainty model was further improved and used for significant tests of TRP measurements [32]. Provided that the K-factor associated with DUT can be estimated, it is possible to reduce the measurement uncertainty of the OTA tests [33]. Unfortunately, the K-factor seen by the DUT is often unknown. In this case, Remley *et al.* [33] developed a method to bound the measurement uncertainty. For accurate implementation of OTA tests, a step-by-step guidance on configuring and verifying the performance of RC-based OTA tests was proposed in [34]. The interested readers can refer to [32]–[34] for detailed study of this topic.

V. CONCLUSION

An overview of nearly two decades of research on RC-based OTA tests was given in this paper. It was shown that free-space characteristics of antennas (i.e., efficiencies, reflection coefficients, and radiation patterns) as well as multipath characterizations of MIMO antennas (i.e., diversity gain, MIMO capacity, and multiplexing efficiency) could be measured in the RC. While most of these parameters can be conveniently measured in the RC, the measurements of radiation pattern and reflection coefficients may not be as good as their counterparts in an AC. Although numerous approaches have been proposed, how to measure the radiation pattern accurately and efficiently in the RC is still an open problem to date. Frequency-, temporal-, and spatial-domain characterizations and their corresponding dualities in the RC were presented. The frequency-temporal characteristic of the channel can be readily controlled to some extent in the RC. More sophisticated channels can be emulated by cascading a CE to the RC. However, there is still limited control of the spatial characteristics at the DUT side. Although it has been experimentally demonstrated that certain amount of anisotropy can be achieved by covering the wall in the RC with absorbers, more efforts should be exerted in investigating to which degree the angular spectrum of the standard MIMO-OTA channel model can be emulated. More importantly, extra caution must be taken in loading the RC so that the measurement uncertainty remains in the acceptable level. Thus, the controllability of the spatial characteristics in the RC remains an unsolved problem. Finally, various active OTA tests were introduced with a special focus on OTA testing of 4G and 5G devices. The RC has been proven to be an efficient tool in measuring the ACLR and CA of base stations. It was shown that the channel could have profound impacts on OTA tests. Therefore, the RC must be carefully calibrated and tuned prior to OTA tests.

REFERENCES

[1] *Electromagnetic Compatibility (EMC), Part 4–21: Testing and Measurement Techniques—Reverberation Chamber Test Methods*, 2nd ed., document IEC 61000-4-21, International Electrotechnical Commission, 2011.

[2] X. Chen, "On statistics of the measured antenna efficiency in a reverberation chamber," *IEEE Trans. Antennas Propag.*, vol. 61, no. 11, pp. 5417–5424, Nov. 2013.

[3] G. L. Fur, P. Besnier, and A. Sharaiha, "Time reversal efficiency measurement in reverberation chamber," *IEEE Trans. Antennas Propag.*, vol. 60, no. 6, pp. 2921–2928, Jun. 2012.

[4] P. Hallbjörner, "Reflective antenna efficiency measurements in reverberation chambers," *Microw. Opt. Technol. Lett.*, vol. 30, no. 5, pp. 332–335, Sep. 2001.

[5] H. G. Krauthäuser and M. Herbrig, "Yet another antenna efficiency measurement method in reverberation chambers," in *Proc. IEEE Int. Symp. Electromagn. Compat.*, Jul. 2010, pp. 536–540.

[6] C. L. Holloway, H. A. Shah, R. J. Pirkl, W. F. Young, D. A. Hill, and J. Ladbury, "Reverberation chamber techniques for determining the radiation and total efficiency of antennas," *IEEE Trans. Antennas Propag.*, vol. 60, no. 4, pp. 1758–1770, Apr. 2012.

[7] C. Li, T.-H. Loh, Z. Tian, Q. Xu, and Y. Huang, "Evaluation of chamber effects on antenna efficiency measurements using non-reference antenna methods in two reverberation chambers," *IET Microw., Antennas Propag.*, vol. 11, no. 11, pp. 1536–1541, 2017.

[8] Q. Xu, Y. Huang, X. Zhu, L. Xing, Z. Tian, and C. Song, "A modified two-antenna method to measure the radiation efficiency of antennas in a reverberation chamber," *IEEE Antennas Wireless Propag. Lett.*, vol. 15, pp. 336–339, 2016.

[9] A. Gifuni, I. D. Flintoft, S. J. Bale, G. C. R. Melia, and A. C. Marvin, "A theory of alternative methods for measurements of absorption cross section and antenna radiation efficiency using nested and contiguous reverberation chambers," *IEEE Trans. Electromagn. Compat.*, vol. 58, no. 3, pp. 678–685, Jun. 2016.

[10] S. J. Boyes, Y. Zhang, A. K. Brown, and Y. Huang, "A method to de-embed external power dividers in efficiency measurements of all-excited antenna arrays in reverberation chamber," *IEEE Antennas Wireless Propag. Lett.*, vol. 11, pp. 1418–1421, 2012.

[11] D. Senic *et al.*, "Improved antenna efficiency measurement uncertainty in a reverberation chamber at millimeter-wave frequencies," *IEEE Trans. Antennas Propag.*, vol. 65, no. 8, pp. 4209–4219, Aug. 2017.

[12] L. K. Warne, K. S. H. Lee, H. G. Hudson, W. A. Johnson, R. E. Jorgenson, and S. L. Stronach, "Statistical properties of linear antenna impedance in an electrically large cavity," *IEEE Trans. Antennas Propag.*, vol. 51, no. 5, pp. 978–992, May 2003.

[13] P.-S. Kildal, C. Carlsson, and J. Yang, "Measurement of free-space impedances of small antennas in reverberation chambers," *Microw. Opt. Technol. Lett.*, vol. 32, no. 2, pp. 112–115, Jan. 2002.

[14] X. Chen and P.-S. Kildal, "Accuracy of antenna input reflection coefficient and mismatch factor measured in reverberation chamber," in *Proc. Eur. Conf. Antennas Propag. (EuCAP)*, Berlin, Germany, Mar. 2009, pp. 2678–2681.

[15] C. Lemoine, E. Amador, P. Besnier, J.-M. Floc'h, and A. Laisné, "Antenna directivity measurement in reverberation chamber from Rician K-factor estimation," *IEEE Trans. Antennas Propag.*, vol. 61, no. 10, pp. 5307–5310, Oct. 2013.

[16] V. Fiumara, A. Fusco, V. Matta, and I. M. Pinto, "Free-space antenna field/pattern retrieval in reverberation environments," *IEEE Antennas Wireless Propag. Lett.*, vol. 4, pp. 329–332, 2011.

[17] P. Besnier, C. Lemonie, J. Sol, and J.-M. Floc'h, "Radiation pattern measurements in reverberation chamber based on estimation of coherent and diffuse electromagnetic fields," in *Proc. IEEE Conf. Antenna Meas. Appl. (CAMA)*, Nov. 2014, pp. 1–4.

[18] M. A. Garcia-Fernandez, D. Carsenat, and C. Decroze, "Antenna radiation pattern measurements in reverberation chamber using plane wave decomposition," *IEEE Trans. Antennas Propag.*, vol. 61, no. 10, pp. 5000–5007, Oct. 2013.

[19] A. Cozza and A. A. el-Aileh, "Accurate radiation-pattern measurements in a time-reversal electromagnetic chamber," *IEEE Trans. Antennas Propag.*, vol. 52, no. 2, pp. 186–193, Apr. 2010.

[20] Q. Xu *et al.*, "3-D antenna radiation pattern reconstruction in a reverberation chamber using spherical wave decomposition," *IEEE Trans. Antennas Propag.*, vol. 65, no. 4, pp. 1728–1739, Apr. 2017.

[21] J. F. Valenzuela-Valdes, M. A. Garcia-Fernandez, A. M. Martinez-Gonzalez, and D. A. Sanchez-Hernandez, "The influence of efficiency on receive diversity and MIMO capacity for Rayleigh-fading channels," *IEEE Trans. Antennas Propag.*, vol. 56, no. 5, pp. 1444–1450, May 2008.

[22] X. Chen, P.-S. Kildal, J. Carlsson, and J. Yang, "MRC diversity and MIMO capacity evaluations of multi-port antennas using reverberation chamber and anechoic chamber," *IEEE Trans. Antennas Propag.*, vol. 61, no. 2, pp. 917–926, Feb. 2013.

[23] Q. Xu, Y. Huang, X. Zhu, S. S. Alja'afreh, and L. Xing, "A new antenna diversity gain measurement method using a reverberation chamber," *IEEE Antennas Wireless Propag. Lett.*, vol. 14, pp. 935–938, 2015.

[24] A. Sorrentino, G. Ferrara, and M. Migliaccio, "The reverberating chamber as a line-of-sight wireless channel emulator," *IEEE Trans. Antennas Propag.*, vol. 56, no. 6, pp. 1825–1830, Jun. 2008.

[25] K. Karlsson, X. Chen, J. Carlsson, and A. Skarbratt, "On OTA test in the presence of Doppler spreads in a reverberation chamber," *IEEE Antennas Wireless Propag. Lett.*, vol. 12, pp. 886–889, 2013.

[26] R. Serra and M. Nabi, "Wireless coexistence and interference test method for low-power wireless sensor networks," *IET Sci. Meas. Technol.*, vol. 9, no. 5, pp. 563–569, 2015.

[27] R. Measel *et al.*, "An empirical study on the performance of wireless OFDM communications in highly reverberant environments," *IEEE Trans. Wireless Commun.*, vol. 15, no. 7, pp. 4802–4812, Jul. 2016.

[28] N. Serafimov, P.-S. Kildal, and T. Bolin, "Comparison between radiation efficiencies of phone antennas and radiated power of mobile phones measured in anechoic chambers and reverberation chamber," in *Proc. IEEE Int. Symp. AP-S*, San Antonio, TX, USA, Jun. 2002, pp. 478–481.

[29] C. Orlenius, P.-S. Kildal, and G. Poilasne, "Measurements of total isotropic sensitivity and average fading sensitivity of CDMA phones in reverberation chamber," in *Proc. IEEE Int. Symp. AP-S*, Jul. 2005, pp. 409–412.

[30] M. Á. García-Fernández, J. D. Sánchez-Heredia, A. M. Martínez-González, D. A. Sánchez-Hernández, and J. F. Valenzuela-Valdés, "Advances in mode-stirred reverberation chambers for wireless communication performance evaluation," *IEEE Commun. Mag.*, vol. 49, no. 7, pp. 140–147, Jul. 2011.

[31] P. S. Kildal, C. Orlenius, and J. Carlsson, "OTA testing in multipath of antennas and wireless devices with MIMO and OFDM," *Proc. IEEE*, vol. 100, no. 7, pp. 2145–2157, Jul. 2012.

[32] K. A. Remley, C.-M. J. Wang, D. F. Williams, J. J. aan den Toorn, and C. L. Holloway, "A significance test for reverberation-chamber measurement uncertainty in total radiated power of wireless devices," *IEEE Trans. Electromagn. Compat.*, vol. 58, no. 1, pp. 207–219, Feb. 2016.

[33] K. A. Remley *et al.*, "Estimating and correcting the device-under-test transfer function in loaded reverberation chambers for over-the-air tests," *IEEE Trans. Electromagn. Compat.*, vol. 59, no. 6, pp. 1724–1733, Dec. 2017.

[34] K. A. Remley *et al.*, "Configuring and verifying reverberation chambers for testing cellular wireless devices," *IEEE Trans. Electromagn. Compat.*, vol. 58, no. 3, pp. 661–672, Jun. 2016.

[35] A. Hussain, P.-S. Kildal, and A. A. Glazunov, "Interpreting the total isotropic sensitivity and diversity gain of LTE-enabled wireless devices from over-the-air throughput measurements in reverberation chambers," *IEEE Access*, vol. 3, pp. 131–145, 2015.

[36] X. Chen, "Throughput modeling and measurement in an isotropic-scattering reverberation chamber," *IEEE Trans. Antennas Propag.*, vol. 62, no. 4, pp. 2130–2139, Apr. 2014.

[37] D. Micheli, M. Barazzetta, F. Moglie, and V. M. Primiani, "Power boosting and compensation during OTA testing of a real 4G LTE base station in reverberation chamber," *IEEE Trans. Electromagn. Compat.*, vol. 57, no. 4, pp. 623–634, Aug. 2015.

[38] M. Barazzetta *et al.*, "A comparison between different reception diversity schemes of a 4G-LTE base station in reverberation chamber: A deployment in a live cellular network," *IEEE Trans. Electromagn. Compat.*, vol. 59, no. 6, pp. 2029–2037, Dec. 2017.

[39] X. Chen, P.-S. Kildal, C. Orlenius, and J. Carlsson, "Channel sounding of loaded reverberation chamber for over-the-air testing of wireless devices: Coherence bandwidth versus average mode bandwidth and delay spread," *IEEE Antennas Wireless Propag. Lett.*, vol. 8, pp. 678–681, 2009.

[40] C. L. Holloway, D. A. Hill, J. M. Ladbury, P. F. Wilson, G. Koepke, and J. Coder, "On the use of reverberation chambers to simulate a Rician radio environment for the testing of wireless devices," *IEEE Trans. Antennas Propag.*, vol. 54, no. 11, pp. 3167–3177, Nov. 2006.

[41] C. S. P. Lötbäck, A. Skårbratt, and C. Orlenius, "Extending the reverberation chamber using a channel emulator for characterisation of over-the-air performance of multiple-input–multiple-output wireless devices," *IET Sci., Meas. Technol.*, vol. 9, no. 5, pp. 555–562, 2015.

[42] C. Wright and S. Basuki, "Utilizing a channel emulator with a reverberation chamber to create the optimal MIMO OTA test methodology," in *Proc. Global Mobile Congr.*, Shanghai, China, Oct. 2010, pp. 1–5.

[43] N. Arsalane *et al.*, "3GPP channel model emulation with analysis of MIMO-LTE performances in reverberation chamber," *Int. J. Antennas Propag.*, vol. 2012, pp. 1–8, Jan. 2012.

[44] J. Kvarnstrand *et al.*, "Mitigation of double-Rayleigh fading when using reverberation chamber cascaded with channel emulator," in *Proc. Eur. Conf. Antennas Propag. (EuCAP)*, London, U.K., Apr. 2018, pp. 1–5.

[45] W. Fan, X. C. B. de Lisbona, F. Sun, J. O. Nielsen, M. B. Knudsen, and G. F. Pedersen, "Emulating spatial characteristics of MIMO channels for OTA testing," *IEEE Trans. Antennas Propag.*, vol. 61, no. 8, pp. 4306–4314, Aug. 2013.

[46] W. Yu, Y. Qi, K. Liu, Y. Xu, and J. Fan, "Radiated two-stage method for LTE MIMO user equipment performance evaluation," *IEEE Trans. Electromagn. Compat.*, vol. 56, no. 6, pp. 1691–1696, Dec. 2014.

[47] *Test Plan for Wireless Large-Form-Factor Device Over-the-Air Performance*, CTIA Certification, Washington, DC, USA, 2016.

[48] K. Rosengren and P.-S. Kildal, "Study of distributions of modes and plane waves in reverberation chambers for the characterization of antennas in a multipath environment," *Microw. Opt. Technol. Lett.*, vol. 30, no. 6, pp. 386–391, Aug. 2001.

[49] M. Otterskog and K. Madsen, "On creating a nonisotropic propagation environment inside a scattered field chamber," *Microw. Opt. Technol. Lett.*, vol. 43, no. 3, pp. 192–195, Nov. 2004.
[50] J. F. Valenzuela-Valdes, A. M. Martinez-Gonzalez, and D. A. Sanchez-Hernandez, "Emulation of MIMO nonisotropic fading environments with reverberation chambers," *IEEE Antennas Wireless Propag. Lett.*, vol. 7, pp. 325–328, 2008.
[51] M. G. Becker *et al.*, "Spatial channels for wireless over-the-air measurements in reverberation chambers," in *Proc. Eur. Conf. Antennas Propag. (EuCAP)*, London, U.K., Apr. 2018, pp. 1–5.
[52] P. S. Kildal, X. Chen, C. Orlenius, M. Franzen, and C. S. L. Patane, "Characterization of reverberation chambers for OTA measurements of wireless devices: Physical formulations of channel matrix and new uncertainty formula," *IEEE Trans. Antennas Propag.*, vol. 60, no. 8, pp. 3875–3891, Aug. 2012.
[53] X. Chen, "Experimental investigation of the number of independent samples and the measurement uncertainty in a reverberation chamber," *IEEE Trans. Electromagn. Compat.*, vol. 55, no. 5, pp. 816–824, Oct. 2013.
[54] X. Chen, "Generalized statistics of antenna efficiency measurement in a reverberation chamber," *IEEE Trans. Antennas Propag.*, vol. 62, no. 3, pp. 1504–1507, Mar. 2014.
[55] D. A. Hill, M. T. Ma, A. R. Ondrejka, B. F. Riddle, M. L. Crawford, and R. T. Johnk, "Aperture excitation of electrically large, lossy cavities," *IEEE Trans. Electromagn. Compat.*, vol. 36, no. 3, pp. 169–178, Aug. 1994.
[56] J. Ladbury and D. A. Hill, "Enhanced backscatter in a reverberation chamber: Inside every complex problem is a simple solution struggling to get out," in *Proc. IEEE Int. Symp. Electromagn. Compat.*, Honolulu, HI, USA, Jul. 2007, pp. 1–5.
[57] C. R. Dunlap, "Reverberation chamber characterization using enhanced backscatter coefficient measurements," Ph.D. dissertation, Dept. Elect., Comput. Energy Eng., Univ. Colorado, Denver, CO, USA, 2013.
[58] Q. Xu *et al.*, "Statistical distribution of the enhanced backscatter coefficient in reverberation chamber," *IEEE Trans. Antennas Propag.*, vol. 66, no. 4, pp. 2161–2164, Apr. 2018.
[59] A. Gifuni, L. Bastianelli, F. Moglie, V. M. Primiani, and G. Gradoni, "Base-case model for measurement uncertainty in a reverberation chamber including frequency stirring," *IEEE Trans. Electromagn. Compat.*, vol. 60, no. 6, pp. 1695–1703, Dec. 2018.
[60] W. Fan, P. Kyösti, Y. Ji, L. Hentilä, X. Chen, and G. F. Pedersen, "Experimental evaluation of user influence on test zone size in multi-probe anechoic chamber setups," *IEEE Access*, vol. 5, pp. 18545–18556, 2017.
[61] A. A. H. Azremi *et al.*, "On Diversity performance of two-element coupling element based antenna structure for mobile terminal," in *Proc. Eur. Conf. Antennas Propag. (EuCAP)*, Barcelona, Spain, Apr. 2010, pp. 1–5.
[62] J. N. Pierce and S. Stein, "Multiple diversity with nonindependent fading," *Proc. IRE*, vol. 48, no. 1, pp. 89–104, 1960.
[63] X. Chen, P.-S. Kildal, and J. Carlsson, "Revisiting the complex correlation in a MIMO system," in *Proc. Eur. Conf. Antennas Propag. (EuCAP)*, Hague, The Netherlands, Apr. 2014, pp. 2735–2739.
[64] S. Blanch, J. Romeu, and I. Corbella, "Exact representation of antenna system diversity performance from input parameter description," *Electron. Lett.*, vol. 39, no. 9, pp. 705–707, May 2003.
[65] P. Hallbjorner, "The significance of radiation efficiencies when using S-parameters to calculate the received signal correlation from two antennas," *IEEE Antennas Wireless Propag. Lett.*, vol. 4, pp. 97–99, 2005.
[66] H. Li, X. Lin, B. K. Lau, and S. He, "Equivalent circuit based calculation of signal correlation in lossy MIMO antennas," *IEEE Trans. Antennas Propag.*, vol. 61, no. 10, pp. 5214–5222, Oct. 2013.
[67] P.-S. Kildal, K. Rosengren, J. Byun, and J. Lee, "Definition of effective diversity gain and how to measure it in a reverberation chamber," *Microw. Opt. Technol. Lett.*, vol. 34, no. 1, pp. 56–59, 2002.
[68] W. Lee, "Mutual coupling effect on maximum-ratio diversity combiners and application to mobile radio," *IEEE Trans. Commun. Technol.*, vol. COM-18, no. 6, pp. 779–791, Dec. 1970.
[69] M. Koohestani, A. Hussain, A. A. Moreira, and A. K. Skrivervik, "Diversity gain influenced by polarization and spatial diversity techniques in ultrawideband," *IEEE Access*, vol. 3, pp. 281–286, 2015.
[70] X. Chen, "Spatial correlation and ergodic capacity of MIMO channel in reverberation chamber," *Int. J. Antennas Propag.*, vol. 2012, pp. 1–7, 2012.
[71] G. Gradoni, X. Chen, T. M. Antonsen, S. M. Anlage, and E. Ott, "Random coupling model for wireless communication channels," in *Proc. EMC Europe*, Gothenburg, Sweden, Sep. 2014, pp. 878–882.
[72] R. He *et al.*, "A kernel-power-density-based algorithm for channel multipath components clustering," *IEEE Trans. Wireless Commun.*, vol. 16, no. 11, pp. 7138–7151, Nov. 2017.
[73] K. Guan *et al.*, "Complete propagation model in tunnels," *IEEE Antennas Wireless Propag. Lett.*, vol. 12, pp. 741–744, 2013.
[74] G. B. Tait and R. E. Richardson, "Wireless channel modeling of multiply connected reverberant spaces: Application to electromagnetic compatibility assessment," *IEEE Trans. Electromagn. Compat.*, vol. 55, no. 6, pp. 1320–1327, Dec. 2013.
[75] L. R. Arnaut and G. Gradoni, "Probability distribution of the coherence bandwidth of a reverberation chamber," *IEEE Trans. Antennas Propag.*, vol. 63, no. 5, pp. 2268–2290, May 2015.
[76] J. N. H. Dortmans, K. A. Remley, D. Senic, C.-M. Wang, and C. L. Holloway, "Use of absorption cross section to predict coherence bandwidth and other characteristics of a reverberation chamber setup for wireless-system tests," *IEEE Trans. Electromagn. Compat.*, vol. 58, no. 5, pp. 1653–1661, Oct. 2016.
[77] C. L. Holloway, H. A. Shah, R. J. Pirkl, K. A. Remley, D. A. Hill, and J. Ladbury, "Early time behavior in reverberation chambers and its effect on the relationships between coherence bandwidth, chamber decay time, RMS delay spread, and the chamber buildup time," *IEEE Trans. Electromagn. Compat.*, vol. 54, no. 4, pp. 714–725, Aug. 2012.
[78] J.-H. Choi, J.-H. Lee, and S.-O. Park, "Characterizing the impact of moving mode-stirrers on the Doppler spread spectrum in a reverberation chamber," *IEEE Antennas Wireless Propag. Lett.*, vol. 9, pp. 375–378, 2010.
[79] K. Karlsson, X. Chen, P.-S. Kildal, and J. Carlsson, "Doppler spread in reverberation chamber predicted from measurements during stepwise stationary stirring," *IEEE Antennas Wireless Propag. Lett*, vol. 9, pp. 497–500, 2010.
[80] L. R. Arnaut, R. Serra, and P. D. West, "Statistical anisotropy in imperfect electromagnetic reverberation," *IEEE Trans. Electromagn. Compat.*, vol. 59, no. 1, pp. 3–13, Feb. 2017.
[81] R. J. Pirkl and K. A. Remley, "Experimental evaluation of the statistical isotropy of a reverberation chamber's plane-wave spectrum," *IEEE Trans. Electromagn. Compat.*, vol. 56, no. 3, pp. 498–509, Jun. 2014.
[82] C. Gentile, A. J. Braga, and A. Kik, "A comprehensive evaluation of joint range and angle estimation in ultra-wideband location systems for indoors," in *Proc. IEEE Int. Conf. Commun. (ICC)*, Beijing, China, May 2008, pp. 4219–4225.
[83] F. Zhang, W. Fan, and G. F. Pedersen, "Frequency-invariant uniform circular array for wideband mm-Wave channel characterization," *IEEE Antennas Wireless Propag. Lett.*, vol. 16, pp. 641–644, 2017.
[84] X. Chen, "Scaling factor for turn-table platform stirring in reverberation chamber," *IEEE Antennas Wireless Propag. Lett.*, vol. 16, pp. 2799–2802, 2017.
[85] *Spatial Channel Model for Multiple Input Multiple Output (MIMO) Simulations*, document 3GPP TR 25.996 V13.0.0, 3rd Generation Partnership Project, Dec. 2015.
[86] P. Corona, G. Ferrara, and M. Migliaccio, "Reverberating chamber electromagnetic field in presence of an unstirred component," *IEEE Trans. Electromagn. Compat.*, vol. 42, no. 2, pp. 111–115, May 2000.
[87] C. Lemoine, E. Amador, and P. Besnier, "On the K-factor estimation for Rician channel simulated in reverberation chamber," *IEEE Trans. Antennas Propag.*, vol. 59, no. 3, pp. 1003–1012, Mar. 2011.
[88] A. Adardour, G. Andrieu, and A. Reineix, "On the low-frequency optimization of reverberation chambers," *IEEE Trans. Electromagn. Compat.*, vol. 56, no. 2, pp. 266–275, Apr. 2014.
[89] X. Chen, "Using Akaike information criterion for selecting the field distribution in a reverberation chamber," *IEEE Trans. Electromagn. Compat.*, vol. 55, no. 4, pp. 664–670, Aug. 2013.
[90] I. Szini, G. F. Pedersen, A. Scannavini, and L. J. Foged, "MIMO 2×2 reference antennas concept," in *Proc. Eur. Conf. Antennas Propag. (EuCAP)*, Prague, Czech Republic, Mar. 2012, pp. 1540–1543.
[91] X. Chen, W. Fan, P. Kyösti, L. Hentilä, and G. F. Pedersen, "Throughput modeling and validations for MIMO-OTA testing with arbitrary multipath," *IEEE Antennas Wireless Propag. Lett.*, vol. 17, no. 4, pp. 637–640, Apr. 2018.
[92] *Multi-Standard Radio (MSR) Base Station (BS) Radio Transmission and Reception, Version 12.6.0*, document 3GPP TS37.104, Dec. 2014.

[93] X. Chen, S. Zhang, and Q. Li, "A review of mutual coupling in MIMO systems," *IEEE Access*, vol. 6, pp. 24706–24719, 2018.
[94] Y. Qi *et al.*, "5G over-the-air measurement challenges: Overview," *IEEE Trans. Electromagn. Compat.*, vol. 59, no. 6, pp. 1661–1670, Dec. 2017.
[95] C. P. Lötbäck, K. Arvidsson, M. Högberg, and M. Gustafsson, "Base station over-the-air testing in reverberation chamber," in *Proc. Eur. Conf. Antennas and Propag. (EuCAP)*, Paris, France, Mar. 2017, pp. 628–632.
[96] M. Barazzetta, C. Carlini, R. Diamanti, V. M. Primiani, and F. Moglie, "Testing of the carrier aggregation mode for a live LTE base station in reverberation chamber," *IEEE Trans. Veh. Technol.*, vol. 66, no. 4, pp. 3024–3033, Apr. 2017.
[97] K. A. Remley, S. J. Floris, H. A. Shah, and C. L. Holloway, "Static and dynamic propagation-channel impairments in reverberation chambers," *IEEE Trans. Electromagn. Compat.*, vol. 53, no. 3, pp. 589–599, Aug. 2011.
[98] F. Moglie and V. M. Primiani, "Analysis of the independent positions of reverberation chamber stirrers as a function of their operating conditions," *IEEE Trans. Electromagn. Compat.*, vol. 53, no. 2, pp. 288–295, May 2011.
[99] C. Lemoine, P. Besnier, and M. Drissi, "Estimating the effective sample size to select independent measurements in a reverberation chamber," *IEEE Trans. Electromagn. Compat.*, vol. 50, no. 2, pp. 227–236, May 2008.
[100] R. J. Pirkl, K. A. Remley, and C. S. L. Patane, "Reverberation chamber measurement correlation," *IEEE Trans. Electromagn. Compat.*, vol. 54, no. 3, pp. 533–545, Jun. 2012.

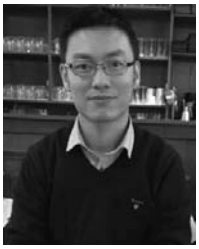

XIAOMING CHEN received the B.Sc. degree in electrical engineering from Northwestern Polytechnical University, Xi'an, China, in 2006, and the M.Sc. and Ph.D. degrees in electrical engineering from the Chalmers University of Technology, Gothenburg, Sweden, in 2007 and 2012, respectively.

From 2013 to 2014, he was a Post-Doctoral Researcher with the Chalmers University of Technology. From 2014 to 2017, he was with Qamcom Research & Technology AB, Gothenburg. Since 2017, he has been a Professor with Xi'an Jiaotong University, Xi'an. His research areas include MIMO antennas, over-the-air testing, reverberation chambers, and hardware impairments and mitigation.

Dr. Chen was a recipient of the 1000-Talent Plan for Young Scholars in China, the Outstanding Associate Editor (AE) Award in 2018, and the International Union of Radio Science Young Scientist Awards in 2017 and 2018. He serves as an AE for the IEEE Antennas and Wireless Propagation Letters.

JIAZHI TANG received the B.S. degree in information engineering from Xi'an Jiaotong University, Xi'an, China, in 2017, where he is currently pursuing the M.S. degree in electronics science and technology.

His research interests include reverberation chamber and mode-stirrer design.

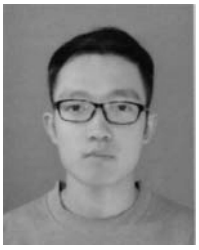

TENG LI received the B.Eng. degree from Northwestern Polytechnical University, Xi'an, China, in 2017. He is currently pursuing the M.Eng. degree with Xi'an Jiaotong University, Xi'an.

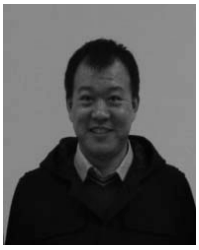

SHITAO ZHU received the B.S. degree in electronic information science and technology from Lanzhou University, Lanzhou, China, in 2005, and the M.S. degree in information and communication engineering and the Ph.D. degree in electronic science and technology from Xi'an Jiaotong University, Xi'an, China, in 2008 and 2016, respectively. He currently holds a post-doctoral position at the Department of Information and Communication Engineering, Xi'an Jiaotong University.

From 2008 to 2012, he was a Systems Engineer with ZTE Co., Ltd., Xi'an. His research interests are in the areas of loop delay estimation, convex optimization, and microwave coincidence imaging.

YUXIN REN received the B.Sc. degree from the University of Science and Technology Beijing, Beijing, China, in 2009, and the M.Sc. degree from the Beijing University of Posts and Telecommunications, Beijing, in 2014. From 2014 to 2016, he was with the Beijing National Railway Research & Design Institute of Signal & Communication as an RF Engineer. Since 2017, he has been a Product Manager with Beijing Hwa-Tech Information System Co., Ltd., where his main work is the reverberation chamber's research and design. His current research interests include 5G base station performance test with CAICT and mm-wave test system in reverberation chamber.

ZHIHUA ZHANG received the B.S. degree in optical electronics from the Huazhong University of Science and Technology and the M.S. degree in communication and electronics system from Beijing Jiaotong University. He was a Manager of the Wireless Solution Division, Agilent, China, where he was in charge of wireless solution development. He is currently leading Beijing Hwa-Tech Information System Co., Ltd., to develop test solutions of 5G and IoT.

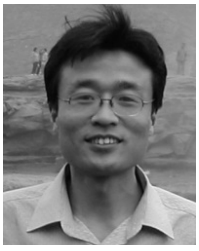

ANXUE ZHANG received the B.S. degree in electrical engineering from Henan Normal University in 1996 and the M.S. and Ph.D. degrees in electromagnetic and microwave engineering from Xi'an Jiaotong University in 1999 and 2003, respectively. He is currently a Professor with Xi'an Jiaotong University. His main research fields include antenna and electromagnetic wave propagation, RF and microwave circuit design, and metamaterials.